Automatica 181 (2025) 112495

Contents lists available at ScienceDirect

Automatica

journal homepage: www.elsevier.com/locate/automatica

Equivariant symmetries for inertial navigation systems ☆

Alessandro Fornasier [a,*], Yixiao Ge [b], Pieter van Goor [c], Robert Mahony [b], Stephan Weiss [a]

[a] Control of Networked Systems Group, University of Klagenfurt, Austria
[b] System Theory and Robotics Lab, Australian Centre for Robotic Vision, Australian National University, Australia
[c] Robotics and Mechatronics group, University of Twente, The Netherlands

ARTICLE INFO

Article history:
Received 8 September 2023
Received in revised form 22 February 2025
Accepted 18 June 2025
Available online 13 August 2025

Keywords:
Inertial navigation system
Symmetry
Equivariance
Equivariant filter

ABSTRACT

This paper investigates the problem of inertial navigation system (INS) filter design through the lens of symmetry. The extended Kalman filter (EKF) and its variants have been the staple of INS filtering for 50 years. However, recent advances in inertial navigation systems have exploited matrix Lie group structure to design stochastic filters and state observers that have been shown to display superior performance compared to classical solutions. In this work, we explore various symmetries of inertial navigation system, including two novel symmetries that have not been considered in the prior literature, and provide a discussion of the relative strengths and weaknesses of these symmetries in the context of filter design. We show that all the modern variants of the EKF for inertial navigation can be interpreted as the recently proposed equivariant filter (EqF) design methodology applied to different choices of symmetry group for the INS problem. As a direct application of the symmetries presented, we address the filter design problem for a vehicle equipped with an inertial measurement unit (IMU) and a global navigation satellite system (GNSS) receiver, providing a comparative analysis of different modern filter solutions. We believe the collection of symmetries that we present here capture all the sensible choices of symmetry for this problem, and that the analysis provided is indicative of the relative real-world performance potential of the different algorithms for trajectories ensuring full state observability.

1. Introduction

The theory of invariant filtering for group affine systems (Barrau, 2015; Barrau & Bonnabel, 2022) and the theory of equivariant filters (Mahony et al., 2020; Ng et al., 2020; Van Goor et al., 2020) that generalizes to systems on homogeneous spaces have provided general design frameworks, as well as strong theoretical performance guarantees, for filter designs that exploit symmetry. This has motivated the widespread use of invariant filters in the robotics community, and its adoption for inertial navigation problems (Hartley et al., 2020; Li et al., 2022; Pavlasek et al., 2021). The application of these principles to inertial navigation systems (INS) has seen the most significant performance gains from algorithm design in this field for the last 40 years. There are now several competing modern INS filters based on geometric insights available in the literature (Barrau & Bonnabel, 2017, 2022; Fornasier et al., 2022b) and the question of how to analyze and evaluate the similarities and differences is now of interest. A recent paper by Barrau et al. states *"The big question when it comes to invariant observers/filters is how do we find a group structure for the state space [...]"* (Barrau & Bonnabel, 2022). The goal of the present paper is to convince the reader that the choice of symmetry structure is in fact the *only* difference between different versions of modern geometric INS filters.

In this paper we present six different symmetry groups that act on the state-space of the INS problem. We use the recent equivariant filter design methodology to generate INS filter algorithms for each of these symmetries. We show that the classical multiplicative extended Kalman filter (MEKF) (Lefferts et al., 1982), the Imperfect-IEKF (Barrau & Bonnabel, 2017), the two-frames group invariant extended Kalman filter (TFG-IEKF) (Barrau & Bonnabel, 2022), and the authors own recent work proposing an equivariant filter for the tangent group structure (TG-EqF) (Fornasier et al., 2022b) are all associated with equivariant filter design (van Goor et al., 2022) applied to different symmetry actions on the same state-space. This leads us to consider the properties of the symmetry groups and suggests two additional symmetries leading to filters, that we term the Direct

☆ The material in this paper was not presented at any conference. This paper was recommended for publication in revised form by Associate Editor Davide Martino Raimondo under the direction of Editor Alessandro Chiuso.

* Corresponding author.
E-mail addresses: alessandro.fornasier@aau.at, alessandrofornasierphd@gmail.com (A. Fornasier), yixiao.ge@anu.edu.au (Y. Ge), p.c.h.vangoor@utwente.nl (P. van Goor), robert.mahony@anu.edu.au (R. Mahony), stephan.weiss@aau.at (S. Weiss).

https://doi.org/10.1016/j.automatica.2025.112495

Position Equivariant Filter (DP-EqF) and Semi-Direct Bias Equivariant Filter (SD-EqF), that are novel and do not correspond to prior algorithms in the literature.

In the context of GNSS-based navigation, we derive EqF algorithms for all of the different symmetries, demonstrating that this approach provides a unifying analysis framework for modern INS filters. In doing this we also make a minor contribution in demonstrating how fixed-frame measurements can be reformulated as body-frame relative measurements. This allows us to exploit output equivariance (van Goor et al., 2022) for all the filter geometries, ensuring at least third-order linearization error in the output equations.

We undertake a simple comparative study in concert with a linearization analysis of the error equations. We consider the "fully observable" case where all states are estimated and are observable for the given system trajectories. We recognize that for specific cases where trajectories lead to unobservable states (e.g., straight-line flight, hovering, etc.) some of the following observations may not hold. For such trajectories we make the following observations:

- The classical MEKF demonstrates noticeable performance limitations compared to the modern filters. In particular, it demonstrates worse transient response and reports significant overconfidence during the transient phase.
- The performance differences in modern filters are primarily visible during the transient phase of error response. The asymptotic behavior of all filters is similar.
- Notwithstanding the above, the asymptotic performance of the TG-EqF appears superior to all other filters demonstrating the best consistency and the lowest error.
- The TG-EqF filter is the only filter with exact linearization of the navigation states; the only nonlinearities occur in the bias states. The authors believe that this property underlies its performance advantage.
- The bias state transient response of the filters with semi-direct bias symmetry (TG-EqF, DP-EqF and SD-EqF) appears superior to that of filters without this geometric structure (MEKF, IEKF and TFG-IEKF).

The study concludes that any of the IEKF, TG-EqF, DP-EqF, and SD-EqF filters are candidates for a high-performance INS filter design. The lower filter error and energy properties of the TG-EqF recommend it as the leading choice for fully observable trajectories.

2. Notation and preliminaries

In this paper bold lowercase letters are used to indicate vector quantities. Bold capital letters are used to indicate matrices. Regular letters are used to indicate elements of a symmetry group.

Frames of reference are denoted as $\{A\}$ and $\{B\}$. Vectors describing physical quantities expressed in a frame of reference $\{A\}$ are denoted by ${}^A\boldsymbol{x}$. Rotation matrices encoding the orientation of a frame of reference $\{B\}$ with respect to a reference $\{A\}$ are denoted by ${}^A\mathbf{R}_B$; in particular, ${}^A\mathbf{R}_B$ expresses a vector ${}^B\boldsymbol{x}$ defined in the $\{B\}$ frame of reference into a vector ${}^A\boldsymbol{x} = {}^A\mathbf{R}_B\,{}^B\boldsymbol{x}$ expressed in the $\{A\}$ frame of reference. Finally, $\mathbf{I}_n \in \mathbb{R}^{n\times n}$ is the $n \times n$ identity matrix, and $\mathbf{0}_{n\times m} \in \mathbb{R}^{n\times m}$ is the $n \times m$ zero matrix.

For all $\boldsymbol{x} \in \mathbb{R}^n$ define the maps:

$$\overline{(\cdot)} : \mathbb{R}^n \to \mathbb{R}^{n+3}, \qquad \boldsymbol{x} \mapsto \overline{\boldsymbol{x}} = \left(\mathbf{0}_{3\times 1}, \boldsymbol{x}\right),$$

$$\underline{(\cdot)} : \mathbb{R}^n \to \mathbb{R}^{n+3}, \qquad \boldsymbol{x} \mapsto \underline{\boldsymbol{x}} = \left(\boldsymbol{x}, \mathbf{0}_{3\times 1}\right).$$

The following Lie groups are used throughout the paper.

$$\mathbf{SO}(3) = \left\{\mathbf{A} \in \mathbb{R}^{3\times 3} \mid \mathbf{A}\mathbf{A}^\top = \mathbf{I}_3,\ \det(\mathbf{A}) = 1\right\},$$

$$\mathbf{SE}(3) = \left\{\begin{bmatrix}\mathbf{A} & \boldsymbol{b}\\ \mathbf{0}_{1\times 3} & 1\end{bmatrix} \in \mathbb{R}^{4\times 4} \mid \mathbf{A} \in \mathbf{SO}(3),\ \boldsymbol{b} \in \mathbb{R}^3\right\},$$

$$\mathbf{SE}_2(3) = \left\{\begin{bmatrix}\mathbf{A} & \boldsymbol{a} & \boldsymbol{b}\\ \mathbf{0}_{1\times 3} & 1 & 0\\ \mathbf{0}_{1\times 3} & 0 & 1\end{bmatrix} \in \mathbb{R}^{5\times 5} \mid \mathbf{A} \in \mathbf{SO}(3),\ \boldsymbol{a}, \boldsymbol{b} \in \mathbb{R}^3\right\}.$$

Their Lie algebras are the tangent spaces at the identities of each group.

For all $X = \left(\mathbf{A}, \boldsymbol{a}, \boldsymbol{b}\right) \in \mathbf{SE}_2(3) \mid \mathbf{A} \in \mathbf{SO}(3), \boldsymbol{a}, \boldsymbol{b} \in \mathbb{R}^3$, define the map:

$$\Omega(\cdot) : \mathbf{SE}_2(3) \to \mathfrak{se}_2(3), \quad \Omega(X) = \left(\mathbf{0}_{3\times 1}, \mathbf{0}_{3\times 1}, \boldsymbol{a}\right)^\wedge \in \mathfrak{se}_2(3).$$

For all $\boldsymbol{p}, \boldsymbol{q}, \boldsymbol{r} \in \mathbb{R}^3 \mid (\boldsymbol{p}, \boldsymbol{q}, \boldsymbol{r}) \in \mathbb{R}^9$, define the map:

$$\Pi(\cdot) : \mathfrak{se}_2(3) \to \mathfrak{se}(3), \quad \Pi\left(\left(\boldsymbol{p}, \boldsymbol{q}, \boldsymbol{r}\right)^\wedge\right) = \left(\boldsymbol{p}, \boldsymbol{q}\right)^\wedge \in \mathfrak{se}(3).$$

In what follows, we recall the concept of symmetry, equivariance, and equivariant filter design. For an introduction to Lie groups and homogeneous spaces in the context of equivariant filter, we refer the reader to the authors' prior work (Fornasier et al., 2022b; Mahony et al., 2020, 2022; van Goor et al., 2022). The extended preprint version of this paper (Fornasier et al., 2025, Appendix A) also provides additional explanation.

2.1. Symmetry equivariance and lifted system

A symmetry of a kinematic system can be seen as a set of transformations that either leave unchanged or change in a structured manner the equations that govern the motion of the system. This is encoded by a transitive group action ϕ of a Lie group $\mathbf{G}$ (also called a *symmetry group*) on the state space $\mathcal{M}$ of a system. Formally, a (right) Lie group action $\phi : \mathbf{G} \times \mathcal{M} \to \mathcal{M}$ is a smooth map satisfying

$$\phi(XY, \xi) = \phi(Y, \phi(X, \xi)), \qquad \phi(I, \xi) = \xi,$$

for all $X, Y \in \mathbf{G}$ and $\xi \in \mathcal{M}$. An action ϕ is said to be *transitive* if for all $\xi_1, \xi_2 \in \mathcal{M}$, there exists $X \in \mathbf{G}$ such that $\phi(X, \xi_1) = \xi_2$.

A symmetry that transforms the equations of motion of a kinematic system in a structured manner encodes *equivariance* of the system. Formally, consider a system $f : \mathbb{L} \to \mathfrak{X}(\mathcal{M})$ as a map from a vector space of inputs $\mathbb{L}$ to vector fields on the state space $\mathcal{M}$; that is, each input $u \in \mathbb{L}$ corresponds to a vector field $f_u \in \mathfrak{X}(\mathcal{M})$ on the state space $\mathcal{M}$. Then f is said to be *equivariant* if

$$\mathrm{d}\phi_X \circ f_u \circ \phi_{X^{-1}} = f_{\psi_X(u)}, \tag{1}$$

$\forall X \in \mathbf{G}, u \in \mathbb{L}$, and for a right-handed group action $\psi : \mathbf{G}\times\mathbb{L} \to \mathbb{L}$ of the group $\mathbf{G}$ on the input space $\mathbb{L}$. Similarly, a symmetry that changes the output in a structured manner encodes *equivariance of the output*. Formally, consider an output map $h : \mathcal{M} \to \mathcal{N}$ where $\mathcal{N}$ is a smooth manifold called the output space. Then h is said to be *equivariant* if

$$h(\phi_X(\xi)) = \rho_X(h(\xi)), \tag{2}$$

$\forall X \in \mathbf{G}, \xi \in \mathcal{M}$, and for a right-handed action of the group $\mathbf{G}$ on the output space $\mathcal{N}$, that is $\rho : \mathbf{G} \times \mathcal{N} \to \mathcal{N}$.

Note that for any fixed $X \in \mathbf{G}$ the actions ϕ, ψ and ρ can be written as diffeomorphisms $\phi_X : \mathcal{M} \to \mathcal{M}$, $\psi_X : \mathbb{L} \to \mathbb{L}$ and $\rho_X : \mathcal{N} \to \mathcal{N}$.

If a system possesses a symmetry $(\mathbf{G}, \phi)$, the Lie group structure of the symmetry group can be exploited to "lift" the system dynamics on the Lie group. That is, with an arbitrary but fixed choice of origin point $\mathring{\xi} \in \mathcal{M}$, defining a geometric structure called "Lift" $\Lambda : \mathcal{M} \times \mathbb{L} \to \mathfrak{g}$ and defining a *lifted system* $\dot{X} = X\Lambda\left(\phi_X(\mathring{\xi}), u\right)$ whose solutions $X(t)$ at time t, project to solutions $\xi(t)$ (Mahony et al., 2020; van Goor et al., 2022).

2.2. Equivariant filter design

For state estimation problems, lifting the system dynamics onto the Lie group translates the problem to that of estimating an element of the symmetry group $\hat{X} \in \mathbf{G}$ such that $\hat{\xi} = \phi(\hat{X}, \mathring{\xi})$, rather than $\hat{\xi} \in \mathcal{M}$ directly. This is not just an "embedding" of the system on the Lie group, but abstracts the estimation problem to the Lie group. Exploiting the symmetry of the kinematic systems allows the definition of a *global error* $e = \phi(\hat{X}^{-1}, \xi) \in \mathcal{M}$, termed *equivariant error* (Van Goor, 2023; van Goor et al., 2022). The EqF is then the state estimation algorithm that results from applying EKF design principles to the (global) error kinematics, linearized about the fixed origin $\mathring{\xi}$.

Let $f : \mathbb{L} \to \mathfrak{X}(\mathcal{M})$ be a system whose state space is a m-dimensional homogeneous space $\mathcal{M}$, and let $h : \mathcal{M} \to \mathcal{N}$ be an output function where the output space is a n-dimensional smooth manifold $\mathcal{N}$. Assume that f and h are equivariant as in Section 2.1. Let $\xi(t) \in \mathcal{M}$ be a trajectory of the system with measurements,

$$\dot{\xi} = f_u(\xi), \qquad y(t_k) = h(\xi(t_k)),$$

where $u(t) \in \mathbb{L}$ is a measured input signal, and the measurements $y(t_k) \in \mathcal{N}$ occur at discrete times $t_1 < t_2 < \cdots$. Choose a fixed origin $\mathring{\xi} \in \mathcal{M}$ and let $\Lambda : \mathcal{M} \times \mathbb{L} \to \mathfrak{g}$ be a lift of the system. Let $\hat{X} \in \mathbf{G}$ denote the observer state and define its dynamics to be

$$\dot{\hat{X}} = \hat{X}\Lambda(\phi(\hat{X}, \mathring{\xi}), u), \quad \hat{X}(t_k^+) = \exp(\Delta(t_k))\hat{X}(t_k^+),$$

where the $\Delta(t_k) \in \mathfrak{g}$ are correction terms that depend on the measurements $y(t_k)$.

The *equivariant error* is defined to be $e := \phi_{\hat{X}^{-1}}(\xi)$. Choose local coordinates of the state space $\vartheta : \mathcal{U}_{\hat{\xi}} \to \mathbb{R}^m$ in a neighborhood $\mathcal{U}_{\hat{\xi}} \subset \mathcal{M}$ of $\mathring{\xi}$, and choose local coordinates of the output space $\delta : \mathcal{U}_{\mathring{y}} \to \mathbb{R}^n$ in a neighborhood $\mathcal{U}_{\mathring{y}} \subset \mathcal{N}$ of $\mathring{y} = h(\mathring{\xi})$. Let $\varepsilon = \vartheta(e)$ denote the local coordinates of the error e. Then the linearized error dynamics and linearized output are (Van Goor et al., 2020)

$$\begin{aligned}
&\dot{\varepsilon} \approx \mathbf{A}_t^0 \varepsilon,\\
&\mathbf{A}_t^0 = \mathrm{D}_e\big|_{\mathring{\xi}} \vartheta(e)\, \mathrm{D}_E\big|_I \phi_{\mathring{\xi}}(E)\, \mathrm{D}_e\big|_{\mathring{\xi}} \Lambda(e, \mathring{u})\, \mathrm{D}_\varepsilon\big|_{\mathbf{0}} \vartheta^{-1}(\varepsilon),\\
&\delta(h(e)) = \delta\left(h\left(\rho(\hat{X}^{-1}, y)\right)\right) \approx \mathbf{C}^0 \boldsymbol{\varepsilon},\\
&\mathbf{C}^0 = \mathrm{D}_y\big|_{\mathring{y}} \delta(y)\, \mathrm{D}_e\big|_{\mathring{\xi}} h(e)\, \mathrm{D}_{\boldsymbol{\varepsilon}}\big|_{\mathbf{0}} \vartheta^{-1}(\boldsymbol{\varepsilon}).
\end{aligned}$$

If no compatible action ψ of the symmetry group on the input space is found, the state matrix can be computed alternatively according to

$$\begin{aligned}
\mathbf{A}_t^0 = {} & \mathrm{D}_e\big|_{\mathring{\xi}} \vartheta(e)\, \mathrm{D}_\xi\big|_{\mathring{\xi}} \phi_{\hat{X}^{-1}}(\xi)\, \mathrm{D}_E\big|_I \phi_{\mathring{\xi}}(E)\\
& \mathrm{D}_\xi\big|_{\phi_{\hat{X}}(\mathring{\xi})} \Lambda(\xi, u)\, \mathrm{D}_e\big|_{\mathring{\xi}} \phi_{\hat{X}}(e)\, \mathrm{D}_{\boldsymbol{\varepsilon}}\big|_{\mathbf{0}} \vartheta^{-1}(\boldsymbol{\varepsilon}).
\end{aligned}$$

Output equivariance can be exploited to derive a linearized output with third order error (van Goor et al., 2022) as follows

$$\begin{aligned}
&\delta(h(e)) = \delta\left(\rho_{\hat{X}^{-1}}(h(\xi))\right) \approx \mathbf{C}^\star \boldsymbol{\varepsilon} + \mathbf{O}(\boldsymbol{\varepsilon}^3),\\
&\mathbf{C}^\star \boldsymbol{\varepsilon} = \frac{1}{2} \mathrm{D}_y\big|_{\mathring{y}} \delta(y) \left(\mathrm{D}_E\big|_I \rho_E(\mathring{y}) + \mathrm{D}_E\big|_I \rho_E\left(\rho_{\hat{X}^{-1}}(y)\right)\right) \varepsilon^\wedge.
\end{aligned}$$

Let $\mathbf{C}$ be either $\mathbf{C}^0$ or $\mathbf{C}^\star$, then the EqF algorithm is

Predict :

$$\begin{aligned}
&\dot{\hat{X}} = \mathrm{dL}_{\hat{X}} \Lambda(\phi_{\mathring{\xi}}(\hat{X}), u),\\
&\dot{\boldsymbol{\Sigma}} = \mathbf{A}_t^0 \boldsymbol{\Sigma} + \boldsymbol{\Sigma} \mathbf{A}_t^{0\top} + \mathbf{Q},
\end{aligned}$$

Update :

$$\begin{aligned}
&\Delta = \mathrm{D}_E\big|_I \phi_{\mathring{\xi}}(E)^\dagger\, \mathrm{d}\vartheta^{-1} \boldsymbol{\Sigma} \mathbf{C}^\top (\mathbf{C} \boldsymbol{\Sigma} \mathbf{C}^\top + \mathbf{R})^{-1} \delta(\rho(\hat{X}^{-1}, y)),\\
&\boldsymbol{\Sigma} = \left(\mathbf{I} - \boldsymbol{\Sigma} \mathbf{C}^\top (\mathbf{C} \boldsymbol{\Sigma} \mathbf{C}^\top + \mathbf{R})^{-1} \mathbf{C}\right) \boldsymbol{\Sigma},\\
&\hat{X} = \exp(\Delta) \hat{X},
\end{aligned}$$

Reset :

$$\boldsymbol{\Sigma} = \exp\left(\boldsymbol{\Gamma}_{\mathrm{d}\phi_{\mathring{\xi}} \Delta}\right) \boldsymbol{\Sigma} \exp\left(\boldsymbol{\Gamma}_{\mathrm{d}\phi_{\mathring{\xi}} \Delta}\right)^\top.$$

where the last equation (Reset) accounts for the distortion of the covariance due to the change of coordinate maps on a non-flat manifold, and is often referred to as *reset step* or *curvature correction* (Ge et al., 2024; Mahony et al., 2022).

The equations above resemble those of continuous–discrete Kalman-like filters, and indeed, the EqF has the same order of computational complexity as any other Kalman-like filter, such as EKF and MEKF.

3. Outline of the paper

The paper is organized as follows. Section 4 introduces the biased inertial navigation system considered. Section 5 introduces and analyzes different symmetries of the biased inertial navigation system under the lens of equivariance. That is, for each symmetry, its equivariance properties, as well as the relation to classical filter design when exploited within the equivariant filter framework, are discussed. In particular, Table 2 provides an summary of the different symmetries considered, with its rightmost column showing the linearized error dynamics when these symmetries are exploited for filter design. Section 6 describes how the linearization error analysis is carried out. For readers who do not wish to replicate the straightforward but tedious calculations required to compute the linearizations, the detailed derivations are provided in the appendix of the extended preprint of this manuscript (Fornasier et al., 2025, Appendix A). Section 7 discussed the problem of unmanned aerial vehicle (UAV) position-based localization as a direct application of the symmetries presented in Section 5. This application serves as a convenient framework to introduce an interesting result in Section 7.1. That is, how global-referenced measurements are reformulated as residual body-referenced measurements that are compatible with the presented symmetries. Finally, Section 7 concludes with an experimental validation of the performance of the different equivariant filters built upon the symmetries discussed in Section 5.

4. The biased inertial navigation problem

Consider a mobile robot equipped with an IMU providing angular velocity and acceleration measurements, as well as other sensors providing partial direct or indirect state measurements (e.g. a GNSS receiver providing position measurements or a magnetometer providing direction measurements). Let $\{G\}$ denote the global inertial frame of reference and $\{I\}$ denote the IMU frame of reference. In non-rotating, flat earth assumption, the deterministic (noise-free) continuous-time biased inertial navigation system is

$$\dot{{}^G\mathbf{R}_I} = {}^G\mathbf{R}_I \left({}^I\boldsymbol{\omega} - {}^I\boldsymbol{b}_\omega\right)^\wedge, \tag{3a}$$

$$\dot{{}^G\boldsymbol{v}_I} = {}^G\mathbf{R}_I \left({}^I\boldsymbol{a} - {}^I\boldsymbol{b}_a\right) + {}^G\boldsymbol{g}, \tag{3b}$$

$$\dot{{}^G\boldsymbol{p}_I} = {}^G\boldsymbol{v}_I, \tag{3c}$$

$$\dot{{}^I\boldsymbol{b}_\omega} = {}^I\boldsymbol{\tau}_\omega, \tag{3d}$$

$$\dot{{}^I\boldsymbol{b}_a} = {}^I\boldsymbol{\tau}_a. \tag{3e}$$

Here, ${}^G\mathbf{R}_I$ denotes the rigid body orientation, and ${}^G\boldsymbol{p}_I$ and ${}^G\boldsymbol{v}_I$ denote the rigid body position and velocity expressed in the $\{G\}$ frame, respectively. These variables are termed the *navigation*

Table 1
Descriptive-lean notation conversion table.

Description	Descriptive notation	Lean notation
Rigid body orientation	${}^{G}\mathbf{R}_{I}$	$\mathbf{R}$
Rigid body velocity	${}^{G}\boldsymbol{v}_{I}$	$\boldsymbol{v}$
Rigid body position	${}^{G}\boldsymbol{p}_{I}$	$\boldsymbol{p}$
Angular velocity measurement	${}^{I}\boldsymbol{\omega}$	$\boldsymbol{\omega}$
Gyroscope bias	${}^{I}\boldsymbol{b}_{\omega}$	$\boldsymbol{b}_{\omega}$
Acceleration measurement	${}^{I}\boldsymbol{a}$	$\boldsymbol{a}$
Accelerometer bias	${}^{I}\boldsymbol{b}_{a}$	$\boldsymbol{b}_{a}$

states. The gravity vector ${}^{G}\boldsymbol{g}$ is expressed in frame $\{G\}$. The gyroscope measurement and accelerometer measurement are written ${}^{I}\boldsymbol{\omega}$ and ${}^{I}\boldsymbol{a}$ respectively. The two biases ${}^{I}\boldsymbol{b}_{\omega}$ and ${}^{I}\boldsymbol{b}_{a}$ are termed the *bias states*. The inputs $\boldsymbol{\tau}_{\omega}$, $\boldsymbol{\tau}_{a}$ are used to model the biases' dynamics, and are zero when the biases are modeled as constant quantities.

The state space is $\mathcal{M} = \mathcal{SO}(3) \times \mathbb{R}^3 \times \mathbb{R}^3 \times \mathbb{R}^3 \times \mathbb{R}^3$ where the 4 copies of $\mathbb{R}^3$ model velocity, position, and angular and acceleration bias, respectively, and $\mathcal{SO}(3)$ is the $\mathbf{SO}(3)$-torsor with rotation matrices representing coordinates of orientation rather than physical rotation of space. Note that the state space itself is not a Lie-group in the EqF formulation. Rather symmetry is modeled as a group action on $\mathcal{M}$, allowing us to consider different symmetries acting on the same INS state. We write an element of the state space, and an element of the input space respectively

$$\xi = \left({}^{G}\mathbf{R}_{I}, {}^{G}\boldsymbol{v}_{I}, {}^{G}\boldsymbol{p}_{I}, {}^{I}\boldsymbol{b}_{\omega}, {}^{I}\boldsymbol{b}_{a}\right) \in \mathcal{M}, \tag{4}$$

$$u = \left({}^{I}\boldsymbol{\omega}, {}^{I}\boldsymbol{a}, {}^{I}\boldsymbol{\tau}_{\omega}, {}^{I}\boldsymbol{\tau}_{a}\right) \in \mathbb{L} \subset \mathbb{R}^{12}. \tag{5}$$

For the sake of clarity of the presentation, in the following sections, we drop subscripts and superscripts from state, input and output variables, and adopt the lean notation defined in Table 1.

5. INS symmetries

Starting with Table 2, we show the relation between INS filters and symmetry group, as well as the differences in the state error linearization of filters built upon those symmetries. In Sections 5.1–5.3, we discuss the symmetry groups that lead to the design of equivariant filters equivalent to the widely-known MEKF, IEKF, and the recently published TFG-IEKF. In Section 5.4 we briefly recall the tangent group recently introduced and exploited for INS in our prior work (Fornasier et al., 2022a, 2022b). In Sections 5.5 and 5.6, we introduce two new symmetry groups for biased inertial navigation Systems. These groups are based on the semi-direct product and aim to address the over-parametrization of bias states introduced in our prior work (Fornasier et al., 2022b).

5.1. Special orthogonal group $\mathbf{G_O} : \mathbf{SO}(3) \times \mathbb{R}^{12}$

Lie group theory was first applied to navigation systems to overcome the limitation and the singularities of using Euler angles as the parametrization of the attitude of a rigid body. Originally formulated on the quaternion group, the modern approach directly models attitude on the Special Orthogonal group $\mathbf{SO}(3)$.

Define the symmetry group $\mathbf{G_O} := \mathbf{SO}(3) \times \mathbb{R}^{12}$, and let $X = (A, a, b, \alpha, \beta) \in \mathbf{G_O}$, where $A \in \mathbf{SO}(3)$, $a, b, \alpha, \beta \in \mathbb{R}^3$. Let $X = (A_X, a_X, b_X, \alpha_X, \beta_X)$, $Y = (A_Y, a_Y, b_Y, \alpha_Y, \beta_Y)$ be two elements of the symmetry group, then the group product is written $XY = (A_X A_Y, a_X + a_Y, b_X + b_Y, \alpha_X + \alpha_Y, \beta_X + \beta_Y)$. The inverse of an element X is given by $X^{-1} = \left(A^{\top}, -a, -b, -\alpha, -\beta\right)$.

Lemma 1. *Define* $\phi : \mathbf{G_O} \times \mathcal{M} \to \mathcal{M}$ *as*

$$\phi(X, \xi) := \left(\mathbf{R}A,\ \boldsymbol{v} + a,\ \boldsymbol{p} + b,\ \boldsymbol{b}_{\omega} + \alpha,\ \boldsymbol{b}_{a} + \beta\right) \in \mathcal{M}. \tag{6}$$

Then, ϕ *is a transitive right group action of* $\mathbf{G_O}$ *on* $\mathcal{M}$.

The existence of a transitive group action of the symmetry group $\mathbf{G_O}$ on the state space $\mathcal{M}$ guarantees the existence of a lift (Mahony et al., 2020).

Theorem 2. *Define the map* $\Lambda : \mathcal{M} \times \mathbb{L} \to \mathfrak{go}$ *by*

$$\Lambda(\xi, u) := \left(\Lambda_1(\xi, u), \ldots, \Lambda_5(\xi, u)\right).$$

where $\Lambda_1 : \mathcal{M} \times \mathbb{L} \to \mathfrak{so}(3)$, *and* $\Lambda_2, \ldots, \Lambda_5 : \mathcal{M} \times \mathbb{L} \to \mathbb{R}^3$ *are given by*

$$\Lambda_1(\xi, u) := \left({}^{I}\boldsymbol{\omega} - {}^{I}\boldsymbol{b}_{\omega}\right)^{\wedge}, \tag{7}$$

$$\Lambda_2(\xi, u) := {}^{G}\mathbf{R}_{I}\left({}^{I}\boldsymbol{a} - {}^{I}\boldsymbol{b}_{a}\right) + {}^{G}\boldsymbol{g}, \tag{8}$$

$$\Lambda_3(\xi, u) := {}^{G}\boldsymbol{v}_{I}, \tag{9}$$

$$\Lambda_4(\xi, u) := {}^{I}\boldsymbol{\tau}_{\omega}, \tag{10}$$

$$\Lambda_4(\xi, u) := {}^{I}\boldsymbol{\tau}_{a}. \tag{11}$$

Then, the Λ *is a lift for the system in Eq. (3) with respect to the symmetry group* $\mathbf{G_O} := \mathbf{SO}(3) \times \mathbb{R}^{12}$.

In the extended preprint (Fornasier et al., 2025, Appendix A), it is shown that an EqF designed using this symmetry results in the well-known MEKF (Lefferts et al., 1982).

5.2. Extended special Euclidean group $\mathbf{G_{ES}} : \mathbf{SE}_2(3) \times \mathbb{R}^6$

Using the extended pose $\mathbf{SE}_2(3)$ group to model the navigation states of the INS problem is one of the major developments in INS filtering in the last 10 years.

Define $\xi = \left(\mathbf{T}, \boldsymbol{b}\right) \in \mathcal{M} := \mathcal{SE}_2(3) \times \mathbb{R}^6$ to be the state space of the system. $\mathbf{T} = \left(\mathbf{R}, \boldsymbol{v}, \boldsymbol{p}\right) \in \mathcal{SE}_2(3)$ is the extended pose (Brossard et al., 2021), which includes the orientation the, velocity and the position of the rigid body, whereas $\boldsymbol{b} = \left(\boldsymbol{b}_{\omega}, \boldsymbol{b}_{a}\right) \in \mathbb{R}^6$ denotes the IMU biases. Let $u = \left(\boldsymbol{w}, \boldsymbol{\tau}\right) \in \mathbb{L} \subseteq \mathbb{R}^{12}$ denote the system input, where $\boldsymbol{w} = \left(\boldsymbol{\omega}, \boldsymbol{a}\right) \in \mathbb{R}^6$ denotes the input given by the IMU readings, and $\boldsymbol{\tau} = \left(\boldsymbol{\tau}_{\omega}, \boldsymbol{\tau}_{a}\right) \in \mathbb{R}^6$ denotes the input for the IMU biases.[1] Define the matrices

$$\mathbf{G} = (\underline{\boldsymbol{g}})^{\wedge} \in \mathfrak{se}_2(3),$$

$$\mathbf{B} = (\underline{\boldsymbol{b}})^{\wedge} \in \mathfrak{se}_2(3), \qquad \mathbf{N} = \begin{bmatrix} \mathbf{0}_{3\times3} & \mathbf{0}_{3\times1} & \mathbf{0}_{3\times1} \\ \mathbf{0}_{1\times3} & 0 & 1 \\ \mathbf{0}_{1\times3} & 0 & 0 \end{bmatrix} \in \mathbb{R}^{5\times5}.$$

$$\mathbf{W} = (\underline{\boldsymbol{w}})^{\wedge} \in \mathfrak{se}_2(3),$$

Then, the system in Eq. (3) may then be written as

$$\dot{\mathbf{T}} = \mathbf{T}(\mathbf{W} - \mathbf{B} + \mathbf{N}) + (\mathbf{G} - \mathbf{N})\mathbf{T}, \tag{12a}$$

$$\dot{\boldsymbol{b}} = \boldsymbol{\tau}. \tag{12b}$$

Define the symmetry group $\mathbf{G_{ES}} := \mathbf{SE}_2(3) \times \mathbb{R}^6$, and let $X = (C, \gamma) \in \mathbf{G_{ES}}$, where $C = (A, a, b) \in \mathbf{SE}_2(3)$, $A \in \mathbf{SO}(3)$, $a, b \in \mathbb{R}^3$, $\gamma \in \mathbb{R}^6$. Let $X = (C_X, \gamma_X)$, $Y = (C_Y, \gamma_Y)$ be two elements of the symmetry group, then the group product is written $XY = (C_X C_Y, \gamma_X + \gamma_Y)$. The inverse of an element X is given by $X^{-1} = \left(C^{-1}, -\gamma\right)$.

[1] The homogeneous Galilean group $\mathbf{HG}(3)$ is isomorphic to $\mathbf{SE}(3)$ but acts on attitude and velocity rather than attitude and position.

Table 2
Qualitative overview of the differences in the presented symmetries when exploited for filter design. The first column indicates the filter that is obtained by applying equivariant filter design methodology with the symmetry in the second column. The third column describes the features of the state error linearization for the specific filter, whereas the rightmost column shows the linearized error dynamics. For readers that do not have time to compute the linearizations themselves, detailed derivations are provided in the extended preprint (Fornasier et al., 2025, Appendix A).

Filter	Symmetry group	State error linearization.	$\mathbf{A} \mid \dot{\boldsymbol{\varepsilon}} \simeq \mathbf{A}\,\boldsymbol{\varepsilon}$
MEKF (Lefferts et al., 1982)	Special Orthogonal group $\mathbf{G_O} : \mathbf{SO}(3) \times \mathbb{R}^{12}$	State-dependent attitude error dynamics. State-dependent and input-dependent velocity error dynamics. Linear time-invariant position error dynamics. Linear time-invariant bias error dynamics	$\dot{\boldsymbol{\varepsilon}}_R \simeq -\hat{\mathbf{R}}\,\boldsymbol{\varepsilon}_{b_\omega} + \mathcal{O}\left(\boldsymbol{\varepsilon}^2\right)$, $\dot{\boldsymbol{\varepsilon}}_v \simeq -\left(\hat{\mathbf{R}}\left(\boldsymbol{a} - \hat{\boldsymbol{b}}_a\right)\right)^\wedge \boldsymbol{\varepsilon}_R - \hat{\mathbf{R}}\,\boldsymbol{\varepsilon}_{b_a} + \mathcal{O}\left(\boldsymbol{\varepsilon}^2\right)$, $\dot{\boldsymbol{\varepsilon}}_p \simeq \boldsymbol{\varepsilon}_v$, $\dot{\boldsymbol{\varepsilon}}_b = \mathbf{0}$.
Imperfect-IEKF (Barrau & Bonnabel, 2017)	Extended Special Euclidean group $\mathbf{G_{ES}} : \mathbf{SE}_2(3) \ltimes \mathbb{R}^6$	State-dependent attitude, position and velocity error dynamics. Linear time-invariant bias error dynamics	$\dot{\boldsymbol{\varepsilon}}_R \simeq -\hat{\mathbf{R}}\,\boldsymbol{\varepsilon}_{b_\omega} + \mathcal{O}\left(\boldsymbol{\varepsilon}^2\right)$, $\dot{\boldsymbol{\varepsilon}}_v \simeq \boldsymbol{g}^\wedge \boldsymbol{\varepsilon}_R - \hat{\boldsymbol{v}}^\wedge \hat{\mathbf{R}}\,\boldsymbol{\varepsilon}_{b_\omega} - \hat{\mathbf{R}}\,\boldsymbol{\varepsilon}_{b_a} + \mathcal{O}\left(\boldsymbol{\varepsilon}^2\right)$, $\dot{\boldsymbol{\varepsilon}}_p \simeq \boldsymbol{\varepsilon}_v - \hat{\boldsymbol{p}}^\wedge \hat{\mathbf{R}}\,\boldsymbol{\varepsilon}_{b_\omega} + \mathcal{O}\left(\boldsymbol{\varepsilon}^2\right)$, $\dot{\boldsymbol{\varepsilon}}_b = \mathbf{0}$.
TFG-IEKF (Barrau & Bonnabel, 2022)	Two-Frames group $\mathbf{G_{TF}} : \mathbf{SO}(3) \ltimes (\mathbb{R}^6 \oplus \mathbb{R}^6)$	Linear time-invariant attitude error dynamics. State-dependent velocity and position error dynamics. State-dependent and input-dependent bias error dynamics	$\dot{\boldsymbol{\varepsilon}}_R \simeq -\boldsymbol{\varepsilon}_{b_\omega}$, $\dot{\boldsymbol{\varepsilon}}_v \simeq \boldsymbol{g}^\wedge \boldsymbol{\varepsilon}_R - \hat{\boldsymbol{v}}^\wedge \boldsymbol{\varepsilon}_{b_\omega} - \boldsymbol{\varepsilon}_{b_a} + \mathcal{O}\left(\boldsymbol{\varepsilon}^2\right)$, $\dot{\boldsymbol{\varepsilon}}_p \simeq \boldsymbol{\varepsilon}_v - \hat{\boldsymbol{p}}^\wedge \boldsymbol{\varepsilon}_{b_\omega} + \mathcal{O}\left(\boldsymbol{\varepsilon}^2\right)$, $\dot{\boldsymbol{\varepsilon}}_{b_\omega} \simeq \left(\hat{\mathbf{R}}\left(\omega - \hat{\boldsymbol{b}}_\omega\right)\right)^\wedge \boldsymbol{\varepsilon}_{b_\omega} + \mathcal{O}\left(\boldsymbol{\varepsilon}^2\right)$, $\dot{\boldsymbol{\varepsilon}}_{b_a} \simeq \left(\hat{\mathbf{R}}\left(\omega - \hat{\boldsymbol{b}}_\omega\right)\right)^\wedge \boldsymbol{\varepsilon}_{b_a} + \mathcal{O}\left(\boldsymbol{\varepsilon}^2\right)$.
TG-EqF (Fornasier et al., 2022b)	Tangent group $\mathbf{G_{TG}} : \mathbf{SE}_2(3) \ltimes \mathfrak{se}_2(3)$	Linear time-invariant attitude, velocity and position error dynamics. State-dependent and input-dependent bias error dynamics	$\dot{\boldsymbol{\varepsilon}}_R \simeq \boldsymbol{\varepsilon}_{b_\omega}$, $\dot{\boldsymbol{\varepsilon}}_v \simeq \boldsymbol{g}^\wedge \boldsymbol{\varepsilon}_R + \boldsymbol{\varepsilon}_{b_a}$, $\dot{\boldsymbol{\varepsilon}}_p \simeq \boldsymbol{\varepsilon}_v + \boldsymbol{\varepsilon}_{b_v}$, $\dot{\boldsymbol{\varepsilon}}_b \simeq \mathbf{ad}^\vee_{(\hat{\boldsymbol{w}}^\wedge + \mathbf{G})}\,\boldsymbol{\varepsilon}_b + \mathcal{O}\left(\boldsymbol{\varepsilon}^2\right)$.
DP-EqF	Direct Position group[a] $\mathbf{G_{DP}} : \mathbf{HG}(3) \ltimes \mathfrak{hg}(3) \times \mathbb{R}^3$	Linear time-invariant attitude and velocity error dynamics. State-dependent and input-dependent position and bias error dynamics	$\dot{\boldsymbol{\varepsilon}}_R \simeq \boldsymbol{\varepsilon}_{b_\omega}$, $\dot{\boldsymbol{\varepsilon}}_v \simeq \boldsymbol{g}^\wedge \boldsymbol{\varepsilon}_R + \boldsymbol{\varepsilon}_{b_a}$, $\dot{\boldsymbol{\varepsilon}}_p \simeq \boldsymbol{\varepsilon}_v - \hat{\boldsymbol{v}}\,\boldsymbol{\varepsilon}_R + \mathcal{O}\left(\boldsymbol{\varepsilon}^2\right)$, $\dot{\boldsymbol{\varepsilon}}_b \simeq \mathbf{ad}^\vee_{(\hat{\boldsymbol{w}}^\wedge + \mathbf{G})}\,\boldsymbol{\varepsilon}_b + \mathcal{O}\left(\boldsymbol{\varepsilon}^2\right)$.
SD-EqF	Semi-Direct Bias group $\mathbf{G_{SD}} : \mathbf{SE}_2(3) \ltimes \mathfrak{se}(3)$	Linear time-invariant attitude and velocity error dynamics. State-dependent position error dynamics. State-dependent and input-dependent bias error dynamics	$\dot{\boldsymbol{\varepsilon}}_R \simeq \boldsymbol{\varepsilon}_{b_\omega}$, $\dot{\boldsymbol{\varepsilon}}_v \simeq \boldsymbol{g}^\wedge \boldsymbol{\varepsilon}_R + \boldsymbol{\varepsilon}_{b_a}$, $\dot{\boldsymbol{\varepsilon}}_p \simeq \boldsymbol{\varepsilon}_v + \hat{\boldsymbol{p}}^\wedge \boldsymbol{\varepsilon}_{b_\omega} + \mathcal{O}\left(\boldsymbol{\varepsilon}^2\right)$, $\dot{\boldsymbol{\varepsilon}}_b \simeq \mathbf{ad}^\vee_{(\hat{\boldsymbol{w}}^\wedge + \mathbf{G})}\,\boldsymbol{\varepsilon}_b + \mathcal{O}\left(\boldsymbol{\varepsilon}^2\right)$.

[a] The homogeneous Galilean group $\mathbf{HG}(3)$ is isomorphic to $\mathbf{SE}(3)$ but acts on attitude and velocity rather than attitude and position.

Lemma 3. *Define* $\phi : \mathbf{G_{ES}} \times \mathcal{M} \to \mathcal{M}$ *as*

$$\phi\left(X, \xi\right) := \left(\mathbf{T}C, \boldsymbol{b} + \gamma\right) \in \mathcal{M}. \tag{13}$$

Then, ϕ *is a transitive right group action of* $\mathbf{G_{ES}}$ *on* $\mathcal{M}$.

Theorem 4. *Define the map* $\Lambda : \mathcal{M} \times \mathbb{L} \to \mathfrak{g}_{\mathbf{ES}}$ *by*

$$\Lambda\left(\xi, u\right) := \left(\Lambda_1\left(\xi, u\right), \Lambda_2\left(\xi, u\right)\right),$$

where $\Lambda_1 : \mathcal{M} \times \mathbb{L} \to \mathfrak{se}_2(3)$, *and* $\Lambda_2 : \mathcal{M} \times \mathbb{L} \to \mathbb{R}^6$ *are given by*

$$\Lambda_1\left(\xi, u\right) := \left(\mathbf{W} - \mathbf{B} + \mathbf{N}\right) + \mathbf{T}^{-1}\left(\mathbf{G} - \mathbf{N}\right)\mathbf{T}, \tag{14}$$

$$\Lambda_2\left(\xi, u\right) := \boldsymbol{\tau}. \tag{15}$$

Then, Λ *is a lift for the system in Eq. (12) with respect to the symmetry group* $\mathbf{G_{ES}} := \mathbf{SE}_2(3) \times \mathbb{R}^6$.

Applying the EqF filter design methodology to this symmetry leads to the Imperfect-IEKF (Barrau, 2015; Barrau & Bonnabel, 2017). Note that ignoring the bias and considering only the navigation states is the original IEKF filter (Barrau & Bonnabel, 2017). The imperfect term comes from breaking the group-affine symmetry of the navigation states by adding the direct product terms for the bias.

5.3. Two-frames group: $\mathbf{G_{TF}} : \mathbf{SO}(3) \ltimes (\mathbb{R}^6 \oplus \mathbb{R}^6)$

The recently published two-frames group invariant extended Kalman filter (Barrau & Bonnabel, 2022) is one approach to address the theoretical issue in the imperfect IEKF for INS where the bias terms are not part of the symmetry structure.

Consider the system in Eq. (12). Define the symmetry group $\mathbf{G_{TF}} := \mathbf{SO}(3) \ltimes (\mathbb{R}^6 \oplus \mathbb{R}^6)$, where $\mathbf{SO}(3)$ acts on two vector spaces of 6 dimensions each defined with respect to two different frames of references. Let $X = (C, \gamma) \in \mathbf{G_{TF}}$, with $C = (A, (a, b)) \in \mathbf{SE}_2(3) := \mathbf{SO}(3) \ltimes \mathbb{R}^6$ such that $A \in \mathbf{SO}(3)$, $(a, b) \in \mathbb{R}^6$. Let, $* : \mathbf{SO}(3) \times \mathbb{R}^{3N} \to \mathbb{R}^{3N}$ be the rotation term introduced in Barrau and Bonnabel (2022), such that $\forall A \in \mathbf{SO}(3)$ and $x = (x_1, \ldots, x_N) \in \mathbb{R}^{3N}$, $A * x = (Ax_1, \ldots, Ax_N)$. Define the group product $XY = (C_X C_Y, \gamma_X + A_X * \gamma_Y)$ The inverse element of the symmetry group writes $X^{-1} = \left(C^{-1}, -A^T * \gamma\right) \in \mathbf{G_{TF}}$.

Lemma 5. *Define* $\phi : \mathbf{G_{TF}} \times \mathcal{M} \to \mathcal{M}$ *as*

$$\phi\left(X, \xi\right) := \left(\mathbf{T}C, A^T * \left(\boldsymbol{b} - \gamma\right)\right) \in \mathcal{M}. \tag{16}$$

Then, ϕ *is a transitive right group action of* $\mathbf{G_{TF}}$ *on* $\mathcal{M}$.

Theorem 6. *Define* $\Lambda_1 : \mathcal{M} \times \mathbb{L} \to \mathfrak{se}_2(3)$ *as*

$$\Lambda_1\left(\xi, u\right) := \left(\mathbf{W} - \mathbf{B} + \mathbf{N}\right) + \mathbf{T}^{-1}\left(\mathbf{G} - \mathbf{N}\right)\mathbf{T}, \tag{17}$$

define $\Lambda_2 : \mathcal{M} \times \mathbb{L} \to \mathbb{R}^6$ *as*

$$\Lambda_2\left(\xi, u\right) := \left(\boldsymbol{b}_\omega^\wedge\left(\boldsymbol{\omega} - \boldsymbol{b}_\omega\right) - \boldsymbol{\tau}_\omega,\ \boldsymbol{b}_a^\wedge\left(\boldsymbol{\omega} - \boldsymbol{b}_\omega\right) - \boldsymbol{\tau}_a\right). \tag{18}$$

Then, the map $\Lambda\left(\xi, u\right) = \left(\Lambda_1\left(\xi, u\right), \Lambda_2\left(\xi, u\right)\right)$ *is a lift for the system in Eq. (12) with respect to the symmetry group* $\mathbf{G_{TF}} := \mathbf{SO}(3) \ltimes (\mathbb{R}^6 \oplus \mathbb{R}^6)$.

In the extended preprint (Fornasier et al., 2025, Appendix A), it is shown that designing and EqF based on this symmetry leads to the recently published TFG-IEKF (Barrau & Bonnabel, 2022).

5.4. Tangent group $\mathbf{G_{TG}} : \mathbf{SE}_2(3) \ltimes \mathfrak{se}_2(3)$

Recent work (Ng et al., 2020, 2019) considered symmetries and EqF filter design on the tangent group $\mathbf{TG}$ of a general Lie-group. Since bias states are closely related to velocities, these ideas can easily be extended symmetries for bias states (Fornasier et al., 2022b).

Define $\xi = \left(\mathbf{T}, \boldsymbol{b}\right) \in \mathcal{M} := \mathcal{SE}_2(3) \times \mathbb{R}^9$ to be the state space of the system. $\mathbf{T} \in \mathcal{SE}_2(3)$ represents the extended pose, whereas $\boldsymbol{b} = \left(\boldsymbol{b}_\omega, \boldsymbol{b}_a, \boldsymbol{b}_v\right) \in \mathbb{R}^9$ represents the IMU biases, and an additional virtual bias $\boldsymbol{b}_v$. Let $u = \left(\boldsymbol{w}, \boldsymbol{\tau}\right) \in \mathbb{L} \subseteq \mathbb{R}^{18}$ denote the system input, where $\boldsymbol{w} = \left(\boldsymbol{\omega}, \boldsymbol{a}, \boldsymbol{v}\right) \in \mathbb{R}^9$ denotes the input given by the IMU readings, and an additional virtual input $\boldsymbol{v}$. Note that

we can set $\boldsymbol{v} = \boldsymbol{b}_v$ such that the original dynamics in Eq. (3) are recovered. $\boldsymbol{\tau} = (\boldsymbol{\tau}_\omega, \boldsymbol{\tau}_a, \boldsymbol{\tau}_v) \in \mathbb{R}^9$ denotes the input for the IMU biases. Define the matrices

$$\mathbf{G} = (\underline{\boldsymbol{g}})^\wedge \in \mathfrak{se}_2(3),$$

$$\mathbf{B} = \boldsymbol{b}^\wedge \in \mathfrak{se}_2(3), \qquad \mathbf{N} = \begin{bmatrix} \mathbf{0}_{3\times3} & \mathbf{0}_{3\times1} & \mathbf{0}_{3\times1} \\ \mathbf{0}_{1\times3} & 0 & 1 \\ \mathbf{0}_{1\times3} & 0 & 0 \end{bmatrix} \in \mathbb{R}^{5\times5}.$$

$$\mathbf{W} = \boldsymbol{w}^\wedge \in \mathfrak{se}_2(3),$$

With these newly defined matrices, the system in Eq. (3) may then be written in compact form as in Eq. (12). Note, however, that the matrices $\mathbf{B}$ and $\mathbf{W}$ are different than those in Eq. (12).

Define the symmetry group $\mathbf{G_{TG}} := \mathbf{SE}_2(3) \ltimes \mathfrak{se}_2(3)$, and let $X = (C, \gamma) \in \mathbf{G_{TG}}$, where $C \in \mathbf{SE}_2(3)$, $\gamma \in \mathfrak{se}_2(3)$. Let $X = (C_X, \gamma_X)$, $Y = (C_Y, \gamma_Y)$ be two elements of the symmetry group, then the group product is written $XY = \left(C_X C_Y, \gamma_X + \mathrm{Ad}_{C_X}[\gamma_Y]\right)$. The inverse of an element X is given by $X^{-1} = \left(C^{-1}, -\mathrm{Ad}_{C^{-1}}[\gamma]\right)$.

Lemma 7. *Define* $\phi : \mathbf{G_{TG}} \times \mathcal{M} \to \mathcal{M}$ *as*

$$\phi(X, \xi) := \left(\mathbf{T}C, \mathbf{Ad}^\vee_{C^{-1}}\left(\boldsymbol{b} - \gamma^\vee\right)\right) \in \mathcal{M}. \tag{19}$$

Then, ϕ *is a transitive right group action of* $\mathbf{G_{TG}}$ *on* $\mathcal{M}$.

From here, we derive a compatible action of the symmetry group $\mathbf{G_{TG}}$ on the input space $\mathbb{L}$ and derive the lift Λ via constructive design as described in Mahony et al. (2020), Van Goor et al. (2020).

Lemma 8. *Define* $\psi : \mathbf{G_{TG}} \times \mathbb{L} \to \mathbb{L}$ *as*

$$\psi(X, u) := \left(\mathbf{Ad}^\vee_{C^{-1}}\left(\boldsymbol{w} - \gamma^\vee\right) + \Omega^\vee\left(C^{-1}\right), \mathbf{Ad}^\vee_{C^{-1}}\boldsymbol{\tau}\right) \in \mathbb{L}. \tag{20}$$

Then, ψ *is a right group action of* $\mathbf{G_{TG}}$ *on* $\mathbb{L}$.

The system in Eq. (12) is equivariant under the actions ϕ in Eq. (19) and ψ in Eq. (20). The existence of a transitive group action of the symmetry group $\mathbf{G_{TG}}$ on the state space $\mathcal{M}$ and the equivariance of the system guarantees the existence of an equivariant lift (Mahony et al., 2020).

Theorem 9. *Define the map* $\Lambda : \mathcal{M} \times \mathbb{L} \to \mathfrak{g}_{\mathbf{TG}}$ *by*

$$\Lambda(\xi, u) := \left(\Lambda_1(\xi, u), \Lambda_2(\xi, u)\right),$$

where $\Lambda_1 : \mathcal{M} \times \mathbb{L} \to \mathfrak{se}_2(3)$, *and* $\Lambda_2 : \mathcal{M} \times \mathbb{L} \to \mathfrak{se}_2(3)$ *are given by*

$$\Lambda_1(\xi, u) := (\mathbf{W} - \mathbf{B} + \mathbf{N}) + \mathbf{T}^{-1}(\mathbf{G} - \mathbf{N})\mathbf{T}, \tag{21}$$

$$\Lambda_2(\xi, u) := \mathrm{ad}_{\boldsymbol{b}}[\Lambda_1(\xi, u)] - \boldsymbol{\tau}^\wedge. \tag{22}$$

Then, Λ *is an equivariant lift for the system in Eq. (12) with respect to the symmetry group* $\mathbf{G_{TG}} := \mathbf{SE}_2(3) \times \mathfrak{se}_2(3)$.

This approach requires the introduction of a new state $\boldsymbol{b}_v$ in order to apply the full $\mathfrak{se}_2(3)$ semi-direct symmetry on the bias states. This new state is entirely virtual, it does not exist in the real system. Since introducing an entirely virtual state just for the sake of the symmetry appears questionable, it is of interest to consider alternative symmetries that try to preserve the semi-direct group structure that models bias interaction, but does not require the additional bias filter state.

5.5. Direct position group $\mathbf{G_{DP}} : \mathbf{HG}(3) \ltimes \mathfrak{hg}(3) \times \mathbb{R}^3$

In this subsection, we investigate a symmetry that does not require the over-parametrization of the state introduced in Fornasier et al. (2022b) given by the addition of a velocity bias state. Specifically, we achieve this by considering a semi-direct product symmetry only on the homogeneous Galilean structure of the state space and an Euclidean symmetry for the position state.

We introduce the term $\mathbf{HG}(3)$ for the *homogeneous Galilean* group. This corresponds to extended pose transformations $\mathbf{SE}_2(3)$ where the spatial translation is zero. That is the symmetry acts on rotation and velocity only with the semi-direct product induced by the $\mathbf{SE}_2(3)$ geometry. The homogeneous Galilean group is isomorphic to $\mathbf{SE}(3)$ in structure, however, since $\mathbf{SE}(3)$ is synonymous with pose transformation we use the $\mathbf{HG}(3)$ notation to avoid confusion.

The first step towards these goals is to introduce a virtual input $\boldsymbol{v}$ and rewrite Eq. (3c) as $\dot{\boldsymbol{p}} = \mathbf{R}\boldsymbol{v} + \boldsymbol{v}$. Note that the input $\boldsymbol{v}$ can be set to zero to recover the original dynamics in Eq. (3).

Define $\xi = \left(\mathbf{T}, \boldsymbol{p}, \boldsymbol{b}\right) \in \mathcal{M} := \mathcal{HG}(3) \times \mathbb{R}^3 \times \mathbb{R}^6$ to be the state space of the system, where $\mathbf{T} = \left(\mathbf{R}, \boldsymbol{v}\right) \in \mathcal{HG}(3)$ includes the orientation and the velocity of the rigid body. Let $u = \left(\boldsymbol{w}, \boldsymbol{v}, \boldsymbol{\tau}\right) \in \mathbb{L} \subseteq \mathbb{R}^{15}$ denote the system input. Define the matrices

$$\mathbf{G} = (\underline{\boldsymbol{g}})^\wedge \in \mathfrak{se}(3), \quad \mathbf{B} = \boldsymbol{b}^\wedge \in \mathfrak{se}(3), \quad \mathbf{W} = \boldsymbol{w}^\wedge \in \mathfrak{se}(3).$$

Then, the system in Eq. (3) may then be written as

$$\dot{\mathbf{T}} = \mathbf{T}(\mathbf{W} - \mathbf{B}) + \mathbf{G}\mathbf{T}, \tag{23a}$$

$$\dot{\boldsymbol{p}} = \mathbf{R}\boldsymbol{v} + \boldsymbol{v}, \tag{23b}$$

$$\dot{\boldsymbol{b}} = \boldsymbol{\tau}. \tag{23c}$$

Define the symmetry group $\mathbf{G_{DP}} := \mathbf{HG}(3) \ltimes \mathfrak{se}(3) \times \mathbb{R}^3$, and let $X = (B, \beta, c) \in \mathbf{G_{DP}}$ with $B = (A, a) \in \mathbf{HG}(3)$ such that $A \in \mathbf{SO}(3)$, $a \in \mathbb{R}^3$. Let $X = (B_X, \beta_X, c_X), Y = (B_Y, \beta_Y, c_Y) \in \mathbf{G_{DP}}$, the group product is written $XY = \left(B_X B_Y, \beta_X + \mathrm{Ad}_{B_X}[\beta_Y], c_X + c_Y\right)$. The inverse of an element $X \in \mathbf{G_{DP}}$ is given by $X^{-1} = \left(B^{-1}, -\mathrm{Ad}_{B^{-1}}[\beta], -c\right) \in \mathbf{G_{DP}}$.

Lemma 10. *Define* $\phi : \mathbf{G_{DP}} \times \mathcal{M} \to \mathcal{M}$ *as*

$$\phi(X, \xi) := \left(\mathbf{T}B, \mathbf{Ad}^\vee_{B^{-1}}\left(\boldsymbol{b} - \beta^\vee\right), \boldsymbol{p} + c\right) \in \mathcal{M}. \tag{24}$$

Then, ϕ *is a transitive right group action of* $\mathbf{G_{DP}}$ *on* $\mathcal{M}$.

We derive a compatible action of the symmetry group $\mathbf{G_{DP}}$ on the input space $\mathbb{L}$.

Lemma 11. *Define* $\psi : \mathbf{G_{DP}} \times \mathbb{L} \to \mathbb{L}$ *as*

$$\psi(X, u) := \left(\mathbf{Ad}^\vee_{B^{-1}}\left(\boldsymbol{w} - \beta^\vee\right), A^T(\boldsymbol{v} - a), \mathbf{Ad}^\vee_{B^{-1}}\boldsymbol{\tau}\right) \in \mathbb{L}. \tag{25}$$

Then, ψ *is a right group action of* $\mathbf{G_{DP}}$ *on* $\mathbb{L}$.

The system in Eq. (23) is equivariant under the actions ϕ in Eq. (24) and ψ in Eq. (25). Therefore, the existence of an equivariant lift is guaranteed.

Theorem 12. *Define the map* $\Lambda : \mathcal{M} \times \mathbb{L} \to \mathfrak{g}_{\mathbf{DP}}$ *by*

$$\Lambda(\xi, u) := \left(\Lambda_1(\xi, u), \Lambda_2(\xi, u), \Lambda_3(\xi, u)\right),$$

where $\Lambda_1 : \mathcal{M} \times \mathbb{L} \to \mathfrak{hg}(3)$, $\Lambda_2 : \mathcal{M} \times \mathbb{L} \to \mathfrak{se}(3)$, *and* $\Lambda_3 : \mathcal{M} \times \mathbb{L} \to \mathbb{R}^3$ *are given by*

$$\Lambda_1(\xi, u) := (\mathbf{W} - \mathbf{B}) + \mathbf{T}^{-1}\mathbf{G}\mathbf{T}, \tag{26}$$

$$\Lambda_2(\xi, u) := \mathrm{ad}_{\boldsymbol{b}^\wedge}[\Lambda_1(\xi, u)] - \boldsymbol{\tau}^\wedge, \tag{27}$$

$$\Lambda_3(\xi, u) := \mathbf{R}\boldsymbol{v} + v. \tag{28}$$

Then, the Λ *is an equivariant lift for the system in Eq. (23) with respect to the symmetry group* $\mathbf{G_{DP}} := \mathbf{HG}(3) \ltimes \mathfrak{hg}(3) \times \mathbb{R}^3$.

The symmetry proposed in this subsection allows for a minimal state parametrization (i.e. absence of over-parametrization of the state with additional state variables). However, the construction comes at the cost of separating the position state from the geometric $\mathbf{SE}_2(3)$ structure and modeling it as a direct product linear space.

5.6. Semi-direct bias group: $\mathbf{G_{SD}}$: $\mathbf{SE}_2(3) \ltimes \mathfrak{se}(3)$

In this subsection, we investigate a symmetry that maintains a minimal state representation (not requiring the introduction of an additional velocity bias state) while keeping the position state within the geometric structure given by $\mathbf{SE}_2(3)$.

Consider the system in Eq. (12). Define the symmetry group $\mathbf{G_{SD}} := \mathbf{SE}_2(3) \ltimes \mathfrak{se}(3)$ with group product $XY = \left(C_X C_Y, \gamma_X + \mathrm{Ad}_{C_X}[\gamma_Y]\right)$ for $X = (C_X, \gamma_X), Y = (C_Y, \gamma_Y) \in \mathbf{G_{SD}}$. Here, for $X = (C, \gamma) \in \mathbf{G_{SD}}$ one has $C = (A, a, b) = (B, b) \in \mathbf{SE}_2(3)$ such that $A \in \mathbf{SO}(3)$, $a, b \in \mathbb{R}^3$, and $B = (A, a) \in \mathbf{HG}(3)$. The element $C \in \mathbf{SE}_2(3)$ in its matrix representation is written

$$C = \left[\begin{array}{ccc:c} A & & a & b \\ \mathbf{0}_{1\times 3} & & 1 & 0 \\ \hdashline \mathbf{0}_{1\times 3} & & 0 & 1 \end{array}\right] = \left[\begin{array}{ccc:c} & B & & b \\ & & & 0 \\ \hdashline \mathbf{0}_{1\times 3} & & 0 & 1 \end{array}\right] \in \mathbf{SE}_2(3).$$

The inverse element is written

$$X^{-1} = \left(C^{-1}, -\mathrm{Ad}_{B^{-1}}[\gamma]\right) \in \mathbf{G_{SD}}.$$

Lemma 13. *Define* $\phi : \mathbf{G_{SD}} \times \mathcal{M} \to \mathcal{M}$ *as*

$$\phi(X, \xi) := \left(\mathbf{T}C, \mathbf{Ad}^{\vee}_{B^{-1}}\left(\boldsymbol{b} - \gamma^{\vee}\right)\right) \in \mathcal{M}. \tag{29}$$

Then, ϕ *is a transitive right group action of* $\mathbf{G_{SD}}$ *on* $\mathcal{M}$.

Theorem 14. *Define* $\Lambda_1 : \mathcal{M} \times \mathbb{L} \to \mathfrak{se}_2(3)$ *as*

$$\Lambda_1(\xi, u) := (\mathbf{W} - \mathbf{B} + \mathbf{N}) + \mathbf{T}^{-1}(\mathbf{G} - \mathbf{N})\mathbf{T}, \tag{30}$$

define $\Lambda_2 : \mathcal{M} \times \mathbb{L} \to \mathfrak{se}(3)$ *as*

$$\Lambda_2(\xi, u) := \mathrm{ad}_{\boldsymbol{b}^{\wedge}}[\Pi(\Lambda_1(\xi, u))] - \boldsymbol{\tau}^{\wedge}, \tag{31}$$

Then, the map $\Lambda(\xi, u) = (\Lambda_1(\xi, u), \Lambda_2(\xi, u))$ *is a lift for the system in Eq. (12) with respect to the symmetry group* $\mathbf{G_{SD}} := \mathbf{SE}_2(3) \ltimes \mathfrak{se}(3)$.

The symmetry proposed in this subsection is a variation of the symmetry defined in our previous work (Fornasier et al., 2022b) that does not require over-parametrization of the state and additional state variables.

6. Linearization error analysis

In Section 5, we present different symmetry groups for the inertial navigation problem. An indicator of the performance of an EqF with a particular symmetry is the order of approximation error in the associated linearization of error dynamics.

For all symmetries, the origin $\mathring{\xi} \in \mathcal{M}$ is chosen to be $\mathring{\xi} := \left(\mathring{\mathbf{R}}, \mathring{\boldsymbol{v}}, \mathring{\boldsymbol{p}}, \mathring{\boldsymbol{b}}_{\omega}, \mathring{\boldsymbol{b}}_{a}\right) = \left(\mathbf{I}_3, \mathbf{0}_{3\times 1}, \mathbf{0}_{3\times 1}, \mathbf{0}_{3\times 1}, \mathbf{0}_{3\times 1}\right)$. Define the local coordinate chart $\vartheta : \mathcal{U}_{\mathring{\xi}} \to \mathbb{R}^n$, to be

$$\vartheta := (\phi_{\mathring{\xi}} \cdot \exp_{\mathbf{G}})^{-1} = \log_{\mathbf{G}} \cdot \phi_{\mathring{\xi}}^{-1}, \tag{32}$$

on a neighborhood of $\mathring{\xi} \in \mathcal{M}$ such that $\log_{\mathbf{G}} \cdot \phi_{\mathring{\xi}}^{-1}$ is bijective. The chart ϑ is always well-defined locally since all group actions considered are free. The local error coordinates are defined by $\varepsilon := \vartheta(e)$, so long as $e := \phi(\hat{X}^{-1}, \xi)$ remains in the domain of definition of ϑ.

In Eq. (32), $\log_{\mathbf{G}}$ denotes the log coordinates on the symmetry group considered. This map is different for each symmetry group. For a product Lie group $\mathbf{G} := \mathbf{G}_1 \times \mathbf{G}_2$, the logarithm is given by $\log_{\mathbf{G}}((A, B)) = (\log_{\mathbf{G}_1}(A), \log_{\mathbf{G}_2}(B))$. When the product groups are Lie groups with well-known exponential maps, then the standard expressions are used (Chirikjian, 2011). For the semi-direct product groups $\mathbf{G} \ltimes \mathfrak{g}$ where $\mathfrak{g}$ is the Lie algebra of $\mathbf{G}$, we will use a matrix realization to compute the exponential and the logarithm algebraically.

In the rightmost column of Table 2, we present the linearization of the state error dynamics associated with each of the symmetries considered. The linearization is expressed in terms of elements $\varepsilon = \log(E) \in \mathfrak{g}$ where the element $E \in \mathbf{G}$ corresponds bijectively to the error $e \in \mathcal{M}$ through the free group action. That is, we solve

$$\mathrm{D}\vartheta^{-1}(\varepsilon)[\dot{\varepsilon}] \approx \frac{\mathrm{d}}{\mathrm{d}t} e = f(\vartheta^{-1}(\varepsilon), u)$$

for $\dot{\varepsilon}$ to first order in ε. Here $\dot{e} = f(e, u)$ is the full error dynamics expressed as a function of e and the input u (Mahony et al., 2022; van Goor et al., 2022). Finally, the filter design follows the procedure outlined in Section 2 and in the authors' earlier works (Fornasier et al., 2022a, 2022b; Mahony et al., 2022; van Goor et al., 2022). The detailed derivation of the error linearization for each symmetry, as well as the related equivariant filters, are provided in the extended preprint (Fornasier et al., 2025, Appendix A).

Barrau and Bonnabel (2017) developed the IEKF for the bias free INS problem and showed that the linearization of the navigation states was exact. This was a significant improvement on the MEKF geometry, where the linearization of the navigation states is not exact, independently of the bias. However, this exact linearization property is lost when bias is added to the INS problem, the system is no longer group affine (Barrau, 2015). Using a direct product geometric structure to add bias leads to the Imperfect-IEKF (Barrau, 2015) and introduces linearization error in the navigation state equations (cf. Table 2). The remaining filters all model coupling between bias and navigation states using semi-direct geometry of some form or other. The TG-EqF is the only filter for which the linearization of the navigation state is exact. In this case, the linearization error is only present in the bias states. The DP-EqF, SD-EqF and TFG-IEKF all have semi-direct geometric coupling between part of their navigation states and the bias states leading to exact or improved linearization where the coupling acts compatibly with the T$\mathbf{G}$ structure.

7. Application: position-based localization

In the present section, we discuss a practical application of the symmetries presented in Section 5, that is UAV position-based localization.

Consider the system in Eq. (3), and consider the output for global position measurements:

$$h(\xi) = \boldsymbol{p} \in \mathbb{R}^3. \tag{33}$$

It is straightforward to verify the $\mathbf{G_{ES}}$, $\mathbf{G_{TG}}$, $\mathbf{G_{SD}}$, $\mathbf{G_{TF}}$ symmetries do not possess output equivariance (Van Goor et al., 2020; van Goor et al., 2022) for global position measurements directly.

7.1. Reformulation of position measurements as equivariant

Here, we show how position measurements can be reformulated as residual body-frame measurements imposing a nonlinear constraint (Julier et al., 2007). The modified measurement is output equivariant with respect to a suitable group action, and the linearization methodology proposed in van Goor et al. (2022) can be applied to generate cubic linearization error in the output.

Lemma 15. *Let* $\boldsymbol{\pi}$ *be a measurement of global position. Define a new measurement model* $h(\xi) \in \mathbb{R}^3$, *describing the body-referenced difference between the measured global position and the position state as follows*

$$h(\xi) = \mathbf{R}^T\left(\boldsymbol{\pi} - \boldsymbol{p}\right) \in \mathbb{R}^3. \tag{34}$$

Let $y = h(\xi) \in \mathcal{N}$ be a measurement defined according to the above model in Eq. (34), define $\rho : \mathbf{G} \times \mathbb{R}^3 \to \mathbb{R}^3$ such that

$$\rho_X(y) := A^T(y - b). \tag{35}$$

Then, the output defined in Eq. (34) is equivariant.

The noise-free value for y is zero and the output innovation $\delta\left(\rho_{\hat{X}^{-1}}(\mathbf{0})\right) = \rho_{\hat{X}^{-1}}(\mathbf{0}) - \boldsymbol{\pi}$ measures the mismatch of the observer state in reconstructing the true state up to noise in the raw measurement $\boldsymbol{\pi}$.

7.2. Experimental evaluation

We document results from a suite of experiments chosen to provide a comparison of the performance of the MEKF, the Imperfect-IEKF, the TFG-IEKF, an EqF based on the $\mathbf{G_{TG}}$ symmetry (Fornasier et al., 2022b) termed TG-EqF, an EqF based on the $\mathbf{G_{DP}}$ symmetry termed DP-EqF, and an EqF based on the $\mathbf{G_{SD}}$ symmetry termed SD-EqF. Moreover, given the global nature of the measurement, we included in the comparison a left-sided Imperfect-IEKF which directly uses the measurement in Eq. (33). Note that each of the aforementioned EqFs have been implemented including the reset step discussed in Section 2, whereas the Imperfect-IEKFs and the TFG-IEKF have been implemented without reset step, according to their original implementation, discussed in Barrau and Bonnabel (2017, 2022) respectively. We undertake two separate experimental analyses. In the first experiment, we undertake a Monte-Carlo simulation of an UAV equipped with an IMU receiving acceleration and angular velocity measurements at 200 Hz and receiving global position measurements at 10 Hz, simulating a GNSS receiver. In the second experiment, we compare all the filters with real data from the INSANE dataset (Brommer et al., 2024).

7.3. UAV flight simulation

In this experiment, we conducted a Monte-Carlo simulation, including four hundred runs of a simulated UAV equipped with an IMU and receiving global position measurements simulating a GNSS receiver. In order to simulate realistic flight conditions, we selected the initial 80 s from four sequences in the Euroc dataset's vicon room (Burri et al., 2016) as reference trajectories. For each sequence, we generated a hundred runs, incorporating synthetic IMU data generated interpolating and differentiating the Vicon poses, and position measurements while varying the initial conditions for the position (distributed normally around zero with 1 m standard deviation per axis) and the attitude (distributed normally around zero with 20° standard deviation per axis). This experiment considers common realistic condition. For application of the semi-direct product symmetries in scenarios of difficult alignment we refer the reader to the authors' related work (Fornasier et al., 2023, 2022a, 2022b; Scheiber et al., 2023).

The ground truth IMU biases are randomly generated every run following a Gaussian distribution with standard deviation of $0.01\text{rad/s}\sqrt{\text{s}}$ for the gyro bias and $0.01\text{m/s}^2\sqrt{\text{s}}$ for the accelerometer bias. To simulate realistic global position measurement, additive Gaussian noise with a standard deviation of 0.2 m per axis is added.

For a fair comparison, we were careful to use the same prior distributions and noise parameters for all filters. This includes accounting for the different scaling and transformations of noise due to the input and state parametrizations for the different geometries. Similarly, each filter shares the same input and output measurement noise covariance adapted to the particular geometry of the filter. The validity of the noise models can be verified in the Average Energy plot (Fig. 1(a)), which plots the average normalized estimation error squared (ANEES) (Li et al., 2012). Here, all filters initialize with unity ANEES, demonstrating that the prior sampling and observer response corresponds to the stochastic prior used, and all filters converge towards unity ANEES as expected from a filter driven by Gaussian noise. All the filters are initialized at the identity (zero attitude, zero position, zero velocity, and zero biases).

The primary plots in Fig. 1(a) show the RMSE values for the navigation states (on the top) and the bias states (on the bottom). It is clear that the MEKF filter demonstrates worse performance than the modern geometric filters. There is little difference visible in the transient and asymptotic error response of the navigation states for the modern filters. The remaining attitude error is due to yaw error. The position and velocity errors converge to the noise limits of the measurement signals. In contrast, there are clear differences visible in the transient response of the bias states. To make the difference in the transient response clearer, Table 3, shows the average RMSE values of each filter for the first 30 s of the trajectory and the percentage improvement of the geometric filters with respect to the MEKF. Additionally, Table 4 shows the time taken by each filter to reach an average RMSE below 10% of the maximum RMSE value. Based on these results, the filters split roughly into three categories: the three filters with semi-direct bias symmetry (TG-EqF, DP-EqF and SD-EqF) which appear to display the best transient response in any state. The IEKFs and TFG-IEKF, which have the $\mathbf{SE}_2(3)$ symmetry but do not use a semi-direct geometry for the bias geometry, have similar bias transient. The accelerometer bias, in particular, is clearly separated from the filters with the semi-direct group symmetry. Finally, the MEKF which suffers from not modeling the $\mathbf{SE}_2(3)$ symmetry at all.

The average energy plot provides an additional important analysis tool. This plot shows the ANEES (Li et al., 2012) defined as

$$\text{ANEES} = \frac{1}{nM}\sum_{i=1}^{M} \boldsymbol{\varepsilon}_i^T \boldsymbol{\Sigma}_i^{-1} \boldsymbol{\varepsilon}_i,$$

where $\boldsymbol{\varepsilon}$ is the specific filter error state, $\boldsymbol{\Sigma}$ is the error covariance, $M = 400$ is the number of runs in the Monte-Carlo simulation, and n is the dimension of the state space. The ANEES provides a measure of the consistency of the filter estimate. An ANEES of unity means that the observed error variance corresponds exactly to the estimated covariance of the information state. When ANEES is larger than unity, it indicates that the filter is overconfident; that is, the observed error is larger than the estimate of the state covariance predicts. All 'pure' extended Kalman filters tend to be overconfident since their derivation ignores linearization errors in the model. The closer to an ANEES of unity that a filter manages is directly correlated to the consistency of the filter estimate and is usually linked to smaller linearization errors. To provide numeric results, we have averaged the ANEES values over the transient and asymptotic sections of the filter response and presented them in Table 5. Here, it is clear that the TG-EqF is superior, with a consistent ANEES for the whole duration of the experiment, the five other filters R-IEKF, L-IEKF TFG-IEKF, DP-EqF and SD-EqF are similar in the transient phase, with the L-IEKF that improves in the asymptotic phase. Finally, the MEKF is worst. The ANEES of the MEKF diverges to over seven before converging, corresponding to an overconfidence of a factor of seven standard deviations in the state error. Such a level of overconfidence is dangerous in a real-world scenario and may indeed lead to divergence of the filter estimate in certain situations. Note

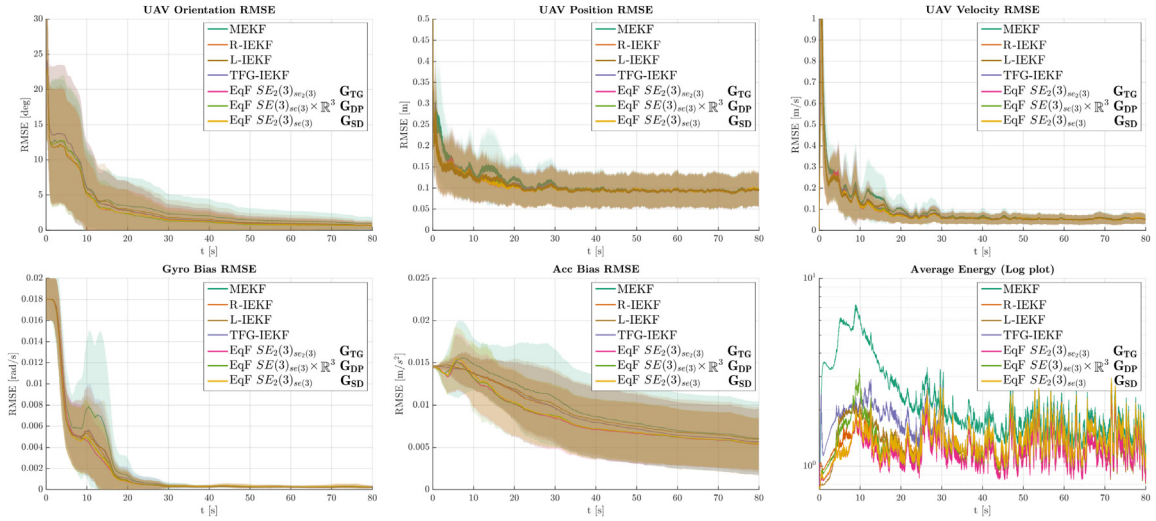

(a) Average RMSE and sample variance (shaded) of the filters' states, and full filter energy.

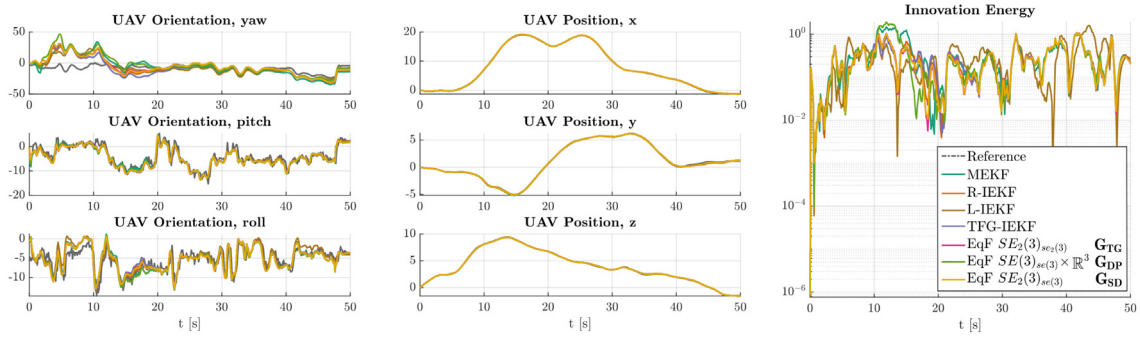

(b) Orientation and position states evolution, and innovation energy for the real-world UAV flight experiment.

Fig. 1. Simulation and real-world experiments' results. Orange: R-IEKF. Brown: L-IEKF. Purple: TFG-IEKF. Magenta: TG-EQF. Green: DP-EQF. Yellow: SD-EQF.

Table 3
RMSE values and percentage of improvement of the geometric filters with respect to the MEKF for the first 30s of the UAV simulation, corresponding to the transient phase (T). Best values are in **bold**, second best values are underlined. In the table, R-IEKF and L-IEKF represent respectively the right-sided and the left-sided Imperfect-IEKF.

RMSE (T)	MEKF	R-IEKF	L-IEKF	TFG-IEKF	TG-EqF	DP-EqF	SD-EqF
Orientation	0.1108 (100%)	0.1076 (97%)	0.1011 (91%)	0.1082 (98%)	**0.0938** (**85**%)	0.0968 (87%)	0.0939 (85%)
Position	0.1433 (100%)	0.1276 (89%)	0.129 (90%)	0.1290 (90%)	0.1267 (88%)	0.1270 (89%)	**0.1263** (**88**%)
Velocity	0.1728 (100%)	0.1459 (84%)	0.146 (84%)	0.1488 (86%)	0.1411 (82%)	0.1411 (82%)	**0.1399** (**81**%)
Gyro bias	0.0054 (100%)	0.0044 (83%)	0.0045 (83%)	0.0046 (85%)	0.0043 (81%)	0.0043 (81%)	**0.0043** (**80**%)
Acc bias	0.0134 (100%)	0.0125 (94%)	0.013 (95%)	0.0126 (94%)	**0.0116** (**87**%)	0.0117 (88%)	0.0119 (89%)

Table 4
Transient times taken by each filter to reach an average RMSE below 10% of the maximum RMSE value. The accelerometer bias is excluded since the average RMSE never reached a value below 10% of the maximum RMSE value. Best values are in **bold**, second best values are underlined. In the table, R-IEKF and L-IEKF represent respectively the right-sided and the left-sided Imperfect-IEKF.

Transient time	MEKF	R-IEKF	L-IEKF	TFG-IEKF	TG-EqF	DP-EqF	SD-EqF
Orientation	32.090 (100%)	23.095 (72%)	26.595 (83%)	23.995 (75%)	21.295 (66%)	**20.395** (**64**%)	21.295 (66%)
Position	5.095 (100%)	4.795 (94%)	**4.595** (**90**%)	4.795 (94%)	4.995 (98%)	4.795 (94%)	4.795 (94%)
Velocity	16.295 (100%)	**12.495** (**77**%)	15.895 (98%)	**12.495** (**77**%)	**12.495** (**77**%)	12.695 (78%)	**12.495** (**77**%)
Gyro bias	17.095 (100%)	16.095 (94%)	16.395 (96%)	16.295 (95%)	**15.895** (**93**%)	16.195 (95%)	**15.895** (**93**%)

that in practice, overconfidence of a filter is avoided by inflating the process noise model covariance to account for linearization error in the model. A more consistent filter requires a smaller covariance inflation and has correspondingly more confidence in its model than a filter that is less consistent.

In conclusion, the TG-EqF exhibits the best convergence rate, particularly in orientation and IMU biases, as well as the best consistency of all the filters. Hence, the TG-EqF is the filter we recommend using for INS problems. We believe that this performance can be traced back to the coupling of the IMU bias with the navigation states that are inherent in the semi-direct product structure of the symmetry group $\mathbf{G_{TG}}$ and the exact linearization of the navigation error dynamics (Table 2). Note that the bias states are poorly observable states and possess slow dynamics.

Table 5
ANEES for the first 30 s, corresponding to the transient phase (T) and for the remaining of the trajectory length, corresponding to the asymptotic phase (A). Best values are in **bold**, second best values are underlined. In the table, R-IEKF and L-IEKF represent respectively the right-sided and the left-sided Imperfect-IEKF.

ANEES	MEKF	R-IEKF	L-IEKF	TFG-IEKF	TG-EqF	DP-EqF	SD-EqF
Transient (T)	3.11	1.36	1.39	1.71	**1.20**	1.44	1.32
Asymptotic (A)	1.69	1.40	**1.20**	1.43	1.22	1.42	1.44

Consequently, moving linearization error into these states heuristically appears better than leaving the linearization error in the main navigation states that are much more dynamic.

7.4. Real-world UAV flight

In this experiment, we compared the performance of the discussed filters in a real-world UAV flight scenario from the INSANE dataset (Brommer et al., 2024). In particular, in this experiment, a quadcopter is flying for 50 m at a maximum height of 13 m covering an area of roughly 200 m^2, at a maximum speed of 3 m/s. The UAV is receiving IMU measurements at 200 Hz, as well as measurements from and RTK-GNSS receiver at 8 Hz with an accuracy between 0.1 m and 0.6 m. The position and orientation reference has been obtained as described in Brommer et al. (2024) from raw sensor measurements of two RTK-GNSS and a magnetometer.

Similar to the previous experiments, all the filters share the same tuning parameters.

Fig. 1(b) shows the evolution of each filter orientation and position estimates, as well as the innovation energy, commonly referred to as the Normalized Innovation Squared (NIS) error

$$\text{NIS} = \frac{1}{n} \boldsymbol{r}^T \mathbf{S}^{-1} \boldsymbol{r},$$

where $\boldsymbol{r}$ is the specific measurement residual of dimension n computed via the output action ρ and $\mathbf{S}$ is the innovation covariance. The results in Fig. 1(b) show that the high level conclusions from the simulations are confirmed on real data. There are slight differences between filters in the plotted results but due to the lack of accurate ground truth all that can be deduced is that all the filters provide high quality real-world INS solutions. This is not surprising since the MEKF is the industry standard and is know to perform well in practice and the more modern filters are expected to improve on this performance.

8. Conclusion

This study investigates inertial navigation system filter design from the perspective of symmetry. We establish a unifying framework, demonstrating that various modern INS filter variants can be interpreted as equivariant filters applied to distinct choices of symmetry, with the group structure being the only difference among those filter variants. With specific application to position measurements, we demonstrated that fixed-frame measurements can be reformulated as body-frame relative measurements. This allows one to exploit the equivariance of the output, ensuring third-order linearization error in the measurement equations.

We discussed and presented different symmetry groups acting on the state-space of the INS problem. Novel symmetries are introduced alongside analysis of similarities and differences in the context of filter design. Furthermore, we showed how different choices of symmetries lead to filters with different linearized error dynamics, and how the $\mathbf{G_{TG}}$ symmetry yields exact linearization of the navigation error, shifting all the linearization error into the bias state dynamics.

Comparative performance studies in simulation, and real-world of a vehicle equipped with an IMU and receiving position measurement from a GNSS receiver highlighted that any of the R-IEKF, L-IEKF, TFG-IEKF, TG-EqF, DP-EqF, and SD-EqF are good candidates for high performance INS filter design with the TG-EqF demonstrating superior performance.

Acknowledgments

The authors would like to thank Martin Scheiber for his invaluable support and insightful discussions, which helped achieve the results presented in the manuscript. The authors would also like to thank the reviewers for their insightful critique that has substantially improved the contribution of the paper.

This work was supported by the BugWright2 EU H2020-Project under the Grant agreement No. 871260 and by the Army Research Office and was accomplished under Cooperative Agreement Number W911NF-21-2-0245.

References

Barrau, Axel (2015). *Non-linear state error based extended Kalman filters with applications to navigation* (Ph.D. thesis), Mines Paristech.

Barrau, A., & Bonnabel, S. (2017). The invariant extended Kalman filter as a stable observer. *IEEE Transactions on Automatic Control*, *62*(4), 1797–1812.

Barrau, Axel, & Bonnabel, Silvere (2022). The geometry of navigation problems. *IEEE Transactions on Automatic Control*, *68*(2), 689–704.

Brommer, Christian, Fornasier, Alessandro, Scheiber, Martin, Delaune, Jeff, Roland, Brockers, Steinbrener, Jan, et al. (2024). The INSANE dataset: Large number of sensors for challenging UAV flights in Mars analog, outdoor, and out-/indoor transition scenarios. *International Journal of Robotics Research*.

Brossard, Martin, Barrau, Axel, Chauchat, Paul, & Bonnabel, Silvere (2021). Associating uncertainty to extended poses for on Lie group IMU preintegration with rotating earth. *IEEE Transactions on Robotics*, *38*(2), 998–1015.

Burri, Michael, Nikolic, Janosch, Gohl, Pascal, Schneider, Thomas, Rehder, Joern, Omari, Sammy, et al. (2016). The EuRoC micro aerial vehicle datasets. *35*, (10), (pp. 1157–1163). http://dx.doi.org/10.1177/0278364915620033.

Chirikjian, Gregory S. (2011). *Analytic methods and modern applications*: *Vol. 2*, *Stochastic models, information theory, and Lie groups*. Springer Science & Business Media.

Fornasier, Alessandro, Ge, Yixiao, van Goor, Pieter, Mahony, Robert, & Weiss, Stephan (2025). Equivariant symmetries for inertial navigation systems. arXiv preprint arXiv:2309.03765.

Fornasier, Alessandro, van Goor, Pieter, Allak, Eren, Mahony, Robert, & Weiss, Stephan (2023). MSCEqF: A multi state constraint equivariant filter for vision-aided inertial navigation. *IEEE Robotics and Automation Letters*.

Fornasier, Alessandro, Ng, Yonhon, Brommer, Christian, Bohm, Christoph, Mahony, Robert, & Weiss, Stephan (2022a). Overcoming bias: Equivariant filter design for biased attitude estimation with online calibration. *IEEE Robotics and Automation Letters*, *7*(4), 12118–12125.

Fornasier, Alessandro, Ng, Yonhon, Mahony, Robert, & Weiss, Stephan (2022b). Equivariant filter design for inertial navigation systems with input measurement biases. In *2022 international conference on robotics and automation* (pp. 4333–4339).

Ge, Yixiao, Van Goor, Pieter, & Mahony, Robert (2024). A geometric perspective on fusing Gaussian distributions on Lie groups. *IEEE Control Systems Letters*, *8*, 844–849.

Hartley, Ross, Ghaffari, Maani, Eustice, Ryan M., & Grizzle, Jessy W. (2020). Contact-aided invariant extended Kalman filtering for robot state estimation. *The International Journal of Robotics Research*, *39*(4), 402–430.

Julier, Simon J., & LaViolar, Joseph J. (2007). On Kalman filtering with nonlinear equality constraints. *IEEE Transactions on Signal Processing*, *55*(6 II), 2774–2784.

Lefferts, E. J., Markley, F. L., & Shuster, M. D. (1982). Kalman filtering for spacecraft attitude estimation. *5*, (5), (pp. 417–429). http://dx.doi.org/10.2514/3.56190.

Li, Xinghan, Jiang, Haodong, Chen, Xingyu, Kong, He, & Wu, Junfeng (2022). Closed-form error propagation on SE-n (3) group for invariant EKF with applications to VINS. *IEEE Robotics and Automation Letters*, *7*(4), 10705–10712.

Mahony, Robert, Hamel, Tarek, & Trumpf, Jochen (2020). Equivariant systems theory and observer design. arXiv preprint arXiv:2006.08276.

Mahony, Robert, Van Goor, Pieter, & Hamel, Tarek (2022). Observer design for nonlinear systems with equivariance. *5*, (pp. 221–252). http://dx.doi.org/10.1146/annurev-control-061520-010324.

Ng, Yonhon, van Goor, Pieter, & Mahony, Robert (2020). Pose observation for second order pose kinematics. *IFAC-PapersOnLine*, *53*(2), 2317–2323.

Ng, Yonhon, Van Goor, Pieter, Hamel, Tarek, & Mahony, Robert (2020). Equivariant systems theory and observer design for second order kinematic systems on matrix Lie groups. In *Proceedings of the IEEE conference on decision and control, 2020-Decem(XX)* (pp. 4194–4199).

Ng, Yonhon, Van Goor, Pieter, Mahony, Robert, & Hamel, Tarek (2019). Attitude observation for second order attitude kinematics. In *Proceedings of the IEEE conference on decision and control, Volume 2019-Decem* (pp. 2536–2542). IEEE.

Pavlasek, Natalia, Walsh, Alex, & Richard Forbes, James (2021). Invariant extended Kalman filtering using two position receivers for extended pose estimation. In *2021 IEEE international conference on robotics and automation* (pp. 5582–5588). Institute of Electrical and Electronics Engineers (IEEE).

Rong Li, X., Zhao, Zhanlue, & Li, Xiao Bai (2012). Evaluation of estimation algorithms: Credibility tests. *IEEE Transactions on Systems, Man, and Cybernetics Part A: Systems and Humans*, *42*(1), 147–163.

Scheiber, Martin, Fornasier, Alessandro, Brommer, Christian, & Weiss, Stephan (2023). Revisiting multi-GNSS navigation for UAVs – An equivariant filtering approach. In *2023 21st international conference on advanced robotics* (pp. 134–141). IEEE.

Van Goor, Pieter (2023). *Equivariant filters for visual spatial awareness* (Ph.D. thesis), Australian National University (ANU).

Van Goor, Pieter, Hamel, Tarek, & Mahony, Robert (2020). Equivariant filter (EqF): A general filter design for systems on homogeneous spaces. In *Proceedings of the IEEE conference on decision and control, 2020-Decem(Cdc)* (pp. 5401–5408).

van Goor, Pieter, Hamel, Tarek, & Mahony, Robert (2022). Equivariant filter (EqF). *IEEE Transactions on Automatic Control*, *68*(6), 3501–3512.

Alessandro Fornasier is currently a senior Robotics Engineer with Hexagon Robotics. He obtained his Ph.D. at the Control of Networked Systems (CNS) group, in 2024, supervised by Stephan Weiss, and Robert Mahony. During his Ph.D. he focused on equivariant system theory and its application in aided inertial localization and multimodal sensor fusion. Prior to this, he receive his B.Sc. and M.Sc. (summa cum laude) at the University of Udine in 2017 and 2019 respectively. His research interests include localization and mapping, sensor fusion, and spatial AI for autonomous systems.

Yixiao Ge received the B.Eng. degree in mechatronics with first class Honors, in 2020 from the Australian National University, Canberra, Australia. He is currently pursuing the Ph.D. degree in robotics and control from the same university. His research interests include applications of Lie-group theory and Riemannian geometry in robotics problems, with a focus on state estimation and filter design.

Pieter van Goor is currently a postdoctoral research fellow with the Robotics and Mechatronics (RAM) group at the university of Twente, supervised by Antonio Franchi and supported by the Marie Sklodowska-Curie Action of the European Research Council. Prior to this, he worked as a research fellow in the Systems Theory and Robotics (STR) group at the Australian National University (ANU) on the development of equivariant systems theory and applications to problems in robotics and control. Pieter completed his Bachelor of Engineering (Research & Development) (Honors) and Bachelor of Science at ANU in 2018, majoring in Mechatronics and Mathematics respectively. His PhD was awarded in 2023, in which he studied equivariant observer design and its application to problems in visual spatial awareness under the supervision of Robert Mahony at the ANU. His research interests include geometric systems theory, state estimation, and perception for robotic systems.

Robert Mahony is a Professor in the Research School of Engineering at the Australian National University. He received his B.Sc. in 1989 (applied mathematics and geology) and his Ph.D. in 1995 (systems engineering) both from the Australian National University. He is a fellow of the IEEE and was president of the Australian Robotics Association from 2008–2011. He was Director of the Research School of Engineering at the Australian National University 2014–2016. His research interests are in non-linear systems theory with applications in robotics and computer vision. He is known for his work in aerial robotics, equivariant observer design, matrix subspace optimization and image based visual servo control.

Stephan Weiss received the Ph.D. degree in robotics from ETH Zurich, Switzerland. He is currently a full professor at the University of Klagenfurt, Austria, where he leads the Control of Networked Systems Group. He was a Research Technologist with the mobility and robotic systems section at the NASA Jet Propulsion Laboratory where he took part in initiating the Ingenuity Mars helicopter project. His research interests include vision-based navigation, visual-inertial state estimation, and autonomous aerial vehicles.